Dynamics of confined water reconstructed from inelastic x-ray scattering measurements of bulk response functions

Robert H. Coridan,[1,2,3,*] Nathan W. Schmidt,[1,2,3] Ghee Hwee Lai,[1,2,3] Peter Abbamonte,[4,5] and Gerard C. L. Wong[1,2,3,†]

[1]*Department of Bioengineering, University of California, Los Angeles, Los Angeles, California 90095, USA*
[2]*Department of Chemistry and Biochemistry, University of California, Los Angeles, Los Angeles, California 90095, USA*
[3]*California NanoSystems Institute, University of California, Los Angeles, Los Angeles, California 90095, USA*
[4]*Department of Physics, University of Illinois at Urbana-Champaign, Urbana, Illinois 61801, USA*
[5]*Seitz Materials Research Laboratory, University of Illinois at Urbana-Champaign, Urbana, Illinois 61801, USA*

Nanoconfined water and surface-structured water impacts a broad range of fields. For water confined between hydrophilic surfaces, measurements and simulations have shown conflicting results ranging from "liquidlike" to "solidlike" behavior, from bulklike water viscosity to viscosity orders of magnitude higher. Here, we investigate how a homogeneous fluid behaves under nanoconfinement using its bulk response function: The Green's function of water extracted from a library of $S(q,\omega)$ inelastic x-ray scattering data is used to make femtosecond movies of nanoconfined water. Between two confining surfaces, the structure undergoes drastic changes as a function of surface separation. For surface separations of ≈ 9 Å, although the surface-associated hydration layers are highly deformed, they are separated by a layer of bulklike water. For separations of ≈ 6 Å, the two surface-associated hydration layers are forced to reconstruct into a single layer that modulates between localized "frozen" and delocalized "melted" structures due to interference of density fields. These results potentially reconcile recent conflicting experiments. Importantly, we find a different delocalized wetting regime for nanoconfined water between surfaces with high spatial frequency charge densities, where water is organized into delocalized hydration layers instead of localized hydration shells, and are strongly resistant to 'freezing' down to molecular distances (<6 Å).

I. INTRODUCTION

An understanding of confined water and structured water has been a fundamental challenge to physics and chemistry and has important consequences in molecular biology and environmental sciences. Examples include ion channels and aquaporins [1,2], clay swelling [3,4], biological tribology [5,6], and "biological water" at protein surfaces [7]. For water confined between hydrophilic surfaces, a broad range of behavior has been observed experimentally. Direct surface forces apparatus (SFA) measurements [8,9] and simulations [10,11] have shown that water and aqueous solutions maintain the viscosity of bulk water down to nanometer-scale confinement. However, similar measurements have shown that the shear viscosity increases by orders of magnitude [12–15], and simulations have indicated an increase in the translational and rotational correlation lifetimes [10,16]. Computational models of water demonstrate a rich phase behavior consistent with solidification [17–19] and dynamical phenomena like shear thinning [10,20] and shear melting and freezing [16]. While such computational water models have provided useful guidance, they are constrained by the limitations of the specific chosen models and their ability to reproduce optimally different aspects of liquid water, such as diffusional, relaxational, and structural properties. Moreover, direct calculation of dynamical and ensemble-averaged structures for water in these confined systems has proven to be computationally intractable.

In this paper, we examine how a bulk, homogeneous fluid is expected to respond to nanoconfinement through its response function. By doing so, we distinguish confinement effects from the termination of a bulk fluid from effects that originate in confinement-induced phase transitions. We have recently shown that the Green's function of water can be extracted from a library of $S(q,\omega)$ data measured over a data range coextensive with the present limits of third generation synchrotron x-ray sources. This Green's function, the bulk density-density response function for water, has been used to generate "nonbulk" water behavior consistent with extant measured computational and experimental results on hydration structure and dynamics [21]. This technique can be generalized to investigate water near extended sources with steric interactions, such as surfaces [22,23]. In fact, it has been previously shown that the spectrum of density fluctuations near hydrophilic surfaces is virtually identical to that of bulk water [24], indicating that the bulk Green's function approach is applicable for these systems. Here, we use the measured Green's function to reconstruct movies of water with 26-fs time resolution and 0.44-Å spatial resolution under boundary conditions consistent with hydrophilic nanoconfinement. Our results are in agreement with both experiments and computer simulations: We confirm the presence of surface-induced hydration structures, modulated by an exponential decrease of order with a decay length comparable to previous measurements. Also in agreement with simulations and experiments [11,25,26], we observe essentially immobile surface-adhesive water density that becomes an integral part of the adjacent surface. Femtosecond movies show that the first hydration shell away from this surface-adhesive layer impinges strongly on nanoconfined water behavior. Between two confining

*Current address: Division of Chemistry and Chemical Engineering, California Institute of Technology, Pasadena, California 91125, USA.
†gclwong@seas.ucla.edu

surfaces, the structure undergoes a sharp transition as a function of surface separation, with qualitative changes that progressively occur as the number of water layers are reduced one by one. For separations of 9 Å (approximately three water molecular thicknesses), the hydration layers are separated by a layer of bulklike water. As the separation is decreased slightly to 6 Å (approximately two water molecular thicknesses), the two surface-associated hydration layers reconstruct into a single layer that modulates between localized "frozen" and delocalized "melted" structures as the surfaces are sheared relative to one another. This crossover, which potentially reconciles seemingly contradictory measurements of nanoconfined water [8,9,13–15], can be understood in terms of interference effects between density fields propagated from the two confining surfaces. Importantly, we find a surprising delocalized wetting regime for water between surfaces with high-spatial-frequency charge densities, where water is organized into a delocalized hydration layer instead of localized hydration shells around discrete hydration sites. In this regime, frustration effects enforce water fluidity down to molecular distances (<6 Å). These results imply that there are two qualitatively distinct types of hydrophilicity at a molecular level.

II. GREEN'S FUNCTION IMAGING OF DYNAMICS

Inelastic x-ray scattering (IXS) is a technique that combines spectroscopy and x-ray scattering to measure the dynamical structure factor $S(q,\omega)$ of condensed systems, which in principle contains all the information in an interacting system via its correlation functions. This technique has been used to study a broad range of systems [27,28]. The recent development of Green's function imaging (GFI) [21,29,30] combined with high-intensity third generation synchrotron sources have allowed ultrafast movies at subangstrom spatial resolution to be made. In our IXS experiment [Fig. 1(a)], photons of initial momentum k_i and energy E_i are incident on a water sample (Millipore, 18 MΩ-cm), and scattered photons at a final momentum k_f and energy E_f are detected. Scanning k_f and E_i yields the measured dynamical structure factor $S(q,\omega)$, where $q = k_f - k_i$ is the momentum transfer and $\omega = E_f - E_i$ is the energy transfer. IXS data for our reconstructions were measured at Beamline ID-28 of the European Radiation Synchrotron Facility (ESRF), with an incident x-ray energy of 21.747 keV ($\delta E \approx 1.7$ meV, Si(11,11,11) reflection). The step size in q of 0.15 Å^{-1} is larger than the q resolution of each measurement (0.03 Å^{-1}). Data from 6.1 to 7.2 Å^{-1} were collected on the same instrument using the higher intensity Si(9,9,9) reflection with incident energy 17.794 keV ($\delta E \approx 3.0$ meV). A complete discussion of the data analysis used to construct the experimental $S(q,\omega)$ can be found in Ref. [21].

The density-density response function $\chi(q,\omega)$ quantifies the nonlocal, dynamical response of a system to an infinitesimal and instantaneous external point charge and is a Green's function that can be used to propagate the effect on the system of a localized time-dependent external charge distribution. We extract this Green's function from $S(q,\omega)$ measurements by applying the fluctuation-dissipation theorem, $\chi''(q,\omega) = -\pi[S(q,\omega) - S(q,-\omega)]$, then extracting the missing real part with causality-enforcing Kramers-Kronig relations. The
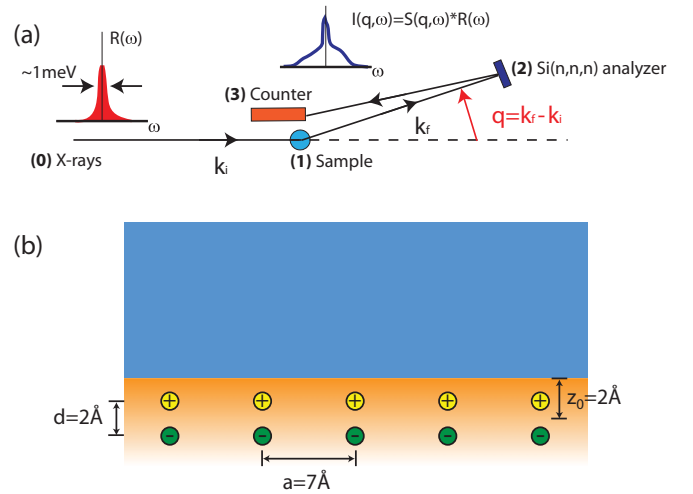

FIG. 1. (Color online) (a) The geometry of the inelastic x-ray scattering experiment: (0) Synchrotron x-rays are conditioned by a monochromator, which reduces their bandwidth to $\delta E \approx 1$ meV. These x rays (initial energy E_i and momentum k_i) are scattered from a sample (1) to an energy discriminating analyzer (2). The analyzer focuses the scattered x rays with final energy E_f and momentum k_f to be counted at a scintillation detector (3). The dynamic structure factor $S(q,\omega)$ is measured as a function of momentum transfer $q = k_f - k_i$ and the energy transfer $\omega = E_f - E_i$. In an IXS experiment, k_i and E_f are fixed, so q and ω are determined by varying the position of the analyzer and incident energy from the monochromator E_i, respectively. The measured intensity $I(q,\omega)$ is the convolution of the physical quantity $S(q,\omega)$ with the instrumental resolution profile $R(\omega)$. (b) We implement a model hydrophilic surface as follows. A square lattice of dipoles (lattice constant $a = 7$ Å) is embedded in a confining surface. (In the diagram, the square lattices of dipoles extend into the page.) Each confining surface is treated as an excluded volume of semi-infinite half-space. The geometrically flat interface which borders this excluded volume represents the idealized model solid-water interface. Each subsurface dipole is composed of charges $\pm q$ separated by $d = 2$ Å (yellow spheres represent positive charges; green spheres represent negative charges), centered at $z_0 = 2$ Å below each solid-water interface. Changing the depth of the dipoles away from the geometric surface does not qualitatively change the results described here.

procedure summarized above for extracting the bulk response function $\chi(q,\omega)$ from IXS measurements of liquid water is described in detail elsewhere. We have recently used this Green's function to reconstruct water dynamics, including the 170-fs dispersive anharmonic oxygen vibrational mode, and diffusional behavior at nanometer scales [21]. The Green's function can be applied to reconstruct the induced charge density $\delta\rho_{ind}(\mathbf{r},t)$ near a dynamical external charge density $\delta\rho_{ext}(\mathbf{r},t)$ by applying the nonlocal dielectric linear response function in energy and momentum-space [31]:

$$\delta\rho_{ind}(\mathbf{q},\omega) = \frac{4\pi^2 e^2}{q^2}\chi(q,\omega)\delta\rho_{ext}(\mathbf{q},\omega). \quad (1)$$

The induced charge density represents the reorganization of water near a dynamical charge distribution.

To reconstruct femtosecond movies of water near a hydrophilic wall, we combine this measured Green's function with a protocol for implementing excluded volume

in polarizable media. A wall is implemented as a charge density embedded in a nonpolarizable ($\epsilon = 1$), slablike cavity. Water is treated as a continuous polarizable medium with its electrodynamics determined by the measured $\chi(q,\omega)$. To make movies of the charge dynamics in this confined water system, we calculate the induced charge density as a function of time. At each calculated time step, the electric displacement field $\mathbf{D}(\mathbf{r},t)$ is calculated from the dynamical external charge density $\delta\rho_{ext}(\mathbf{r},t)$. The polarization field in the water is reconstructed from propagating the electric displacement field with the nonlocal dielectric function at all points in the periodic calculation volume,

$$P_\alpha(\mathbf{q},\omega) = \frac{4\pi^2 e^2}{q^2}\chi(q,\omega)\frac{q_\alpha q_\beta}{q^2}D_\beta(\mathbf{q},\omega), \qquad (2)$$

with an implicit sum over the components of the electric displacement field D_β. The excluded volume is enforced by subtracting the nonlocal contribution to the polarization at all points in the solvent from all points in the wall volume. The water induced charge density $\delta\rho_{ind}(\mathbf{r},t)$ is calculated as the divergence of the induced polarization field, $\delta\rho_{ind}(\mathbf{r},t) = -\nabla \cdot \mathbf{P}_{ind}(\mathbf{r},t)$. For practicality and efficiency this calculation was carried out in a discretized, three-dimensional lattice with periodic boundary conditions, representing the water channel and the excluded volume. The excluded-volume regions were extended for a distance larger than the influence of the response function (>4 nm) to ensure that the water region was isolated from the influence of periodicity in the confining direction. Fast Fourier transforms were used to calculate the momentum-space linear response function, Eq. (2). Further details of this procedure are described elsewhere [22]. It is important to note that although real surfaces are rougher than idealized geometric surfaces, and that the surface structuring of the first water layer is therefore smoother here than that near real surfaces, the dynamics of all subsequent hydration layers are captured by the measured water-water interactions contained in the Green's function from inelastic x-ray scattering.

III. RESULTS

A. Static reconstructions

Before we investigate water confined between two hydrophilic surfaces, we first examine the hydration near a single hydrophilic surface. A schematic of our model surface is shown in Fig. 1(b). The surface hydration structures reconstructed from the measured Green's function are consistent with existing measurements and simulations [10,11,13]. We compare the hydration structure of a surface with an isolated dipole with that from a surface with a square lattice of dipoles (lattice constant $a = 7$ Å, approximately representative of the charge spacing on a mica surface); each dipole is composed of charges $\pm q$ separated by $d = 2$ Å, centered at $y_0 = 2$ Å below the solid-water interface, and oriented so that the dipole moment was normal to the interface. We find that changing the charge separation or the distance between charges and the surface has little qualitative effect on the results. For this model surface, we use the magnitude of q to be the elementary electronic charge, which also approximates the charge density of a mica surface. Because we are using linear response, the value of q only scales the induced charge density. We
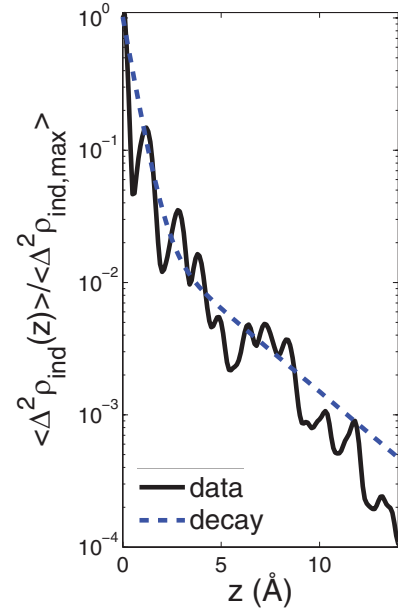

FIG. 2. (Color online) The dependence of the variance of the induced density on the distance from the surface. The variance was chosen to highlight the decay of surface-induced structure. The raw data (solid black line) and two exponential fit (dashed blue line) show that near the surface, the decay of the density is sharp ($\lambda_{ad} \approx 0.5$ Å). This is due to the density fluctuations representing water adhered to the interaction site. For larger distances, the variance decreases with a decay length of $\lambda \approx 3.5$ Å, indicating that the influence of the surface on local density ordering of water is only strong in the first few molecular layers and is nearly zero for $z > 10$ Å.

concentrate on the structure and dynamics of the confined reconstructions in the present model as a function of the gap width between the confining surfaces. The hydration structure near the solid surface was reconstructed from the Green's function using excluded-volume methods described above [22].

From direct inspection, it can be seen that the surface-induced ordering decays away from the surface. The variance of the induced density changes $\Delta^2\rho_{ind}(z)$, calculated from the data by integrating the square of the induced charge density $\delta\rho_{ind}(x,y,z)$ in 0.2-Å xy slices along the z direction (Fig. 2), measures the influence of the surface on density fluctuations as a function of the distance from the interface. It should be noted that although the result in Fig. 2 is integrated in xy slices, the curve is not a simple oscillatory function with a single period because it contains more structural information than similar one-dimensional plots of this type. This is due to the high spatial resolution of the measurement, which is sensitive to the effects of curvature in complex, nonspherical hydration structures.

To quantify approximately the decay of surface-induced ordering in a manner that is independent of the molecular details of hydration shells, a superposition of exponential functions is fit directly to the variance. We find that a sum of two exponential functions with least-squares determined decay lengths of $\lambda_{ad} = 0.5$ Å and $\lambda = 3.5$ Å provide satisfactory fits to describe the decay. λ_{ad} describes the density adjacent to the solid surface and contains information on submolecular

variations of oxygen density in the surface-adhesive water commonly seen in simulations. In contrast, $\lambda = 3.5$ Å governs the longitudinal decay of order in the molecular layers of water away from the solid surface and shows that surface-induced ordering is felt by water for only a few molecular layers. The induced density fluctuations are indistinguishable from bulk water for $z > 1$ nm. These above results on the decay of surface order from our reconstructions are consistent with recent interfacial measurements and simulations [11,15,25,32].
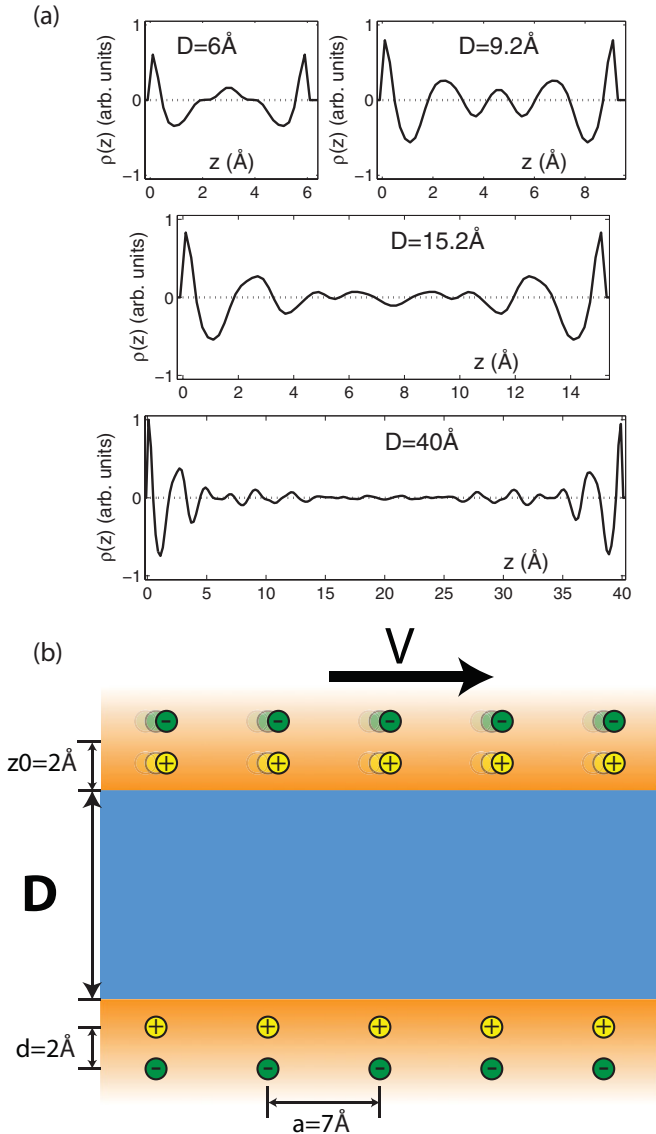

FIG. 3. (Color online) (a) Density $\Delta\rho(z)$ for liquid water confined by hydrophilic surfaces. For subnanometer confinement ($D = 6$ Å, $D = 9.2$ Å), density oscillations about the bulk density (dotted line) can be observed. For larger gaps ($D = 15.2$ Å, $D = 40$ Å), the density oscillations are localized near each surface, with nearly constant bulk densities in the center of the gap. The vertical scale is linear and measured in identical units for all four plots. (b) Confinement is implemented as two single sheets from Fig. 1(b) separated by a distance D. Shear is induced by moving the top interface relative to the bottom interface at V. We assume that the response function of the bulk fluid is not altered by the shear.

We next examine the structure of water confined between two stationary hydrophilic surfaces. Hydration structures for different gap widths D were individually reconstructed from the Green's function using two of the model surfaces described above. The hydration environment between stationary confining surfaces is shown in Fig. 3(a). In this two-dimensional representation, the density between the surfaces is integrated: $\delta\rho_{ind}(z) = \int \delta\rho_{ind}(x,y,z)dxdy$. For large gaps ($D = 15.2$ Å, $D = 40$ Å), pronounced surface-induced density variations only exist near the solid surfaces. The water density midgap (dashed line) is essentially identical to that of bulk water. For these large values of D, the dipole surfaces are sufficiently separated to have nearly independent hydration structures, similar to those observed for single-surface hydration above. For subnanometer confinement ($D = 6$ Å, $D = 9.2$ Å), well-defined hydration layers appear, with induced density oscillations at a spacing of ≈ 3 Å. These results indicate that water can be ordered via cooperative restructuring of water by the two surfaces, and they agree with many computer simulations [11,26].

B. Shearing reconstructions

Cooperativity and frustration between structure-inducing effects from the two confining surfaces as one is sheared past the other lead to drastic differences in the dynamics of nanoconfined water as a function of surface separation D. Here, we make the simplest assumption that shearing does not change the nature of the fluid, and that shear does not change the fluid response in a fundamental way. Shearing is implemented by moving the charge density of the top surface in the periodic calculation volume while keeping the charge density of the bottom surface and the excluded volume constant in time [Fig. 3(b)]. For large separations ($D \gg 10$ Å), cooperative deformations induced by the two bounding surfaces are too weak to be measurable, and the hydration structures near the lattice sites are essentially identical to those for a single surface. For smaller surface separations, hydration structures deform as they optimize their structures to the changing boundary conditions on the two surfaces.

Previous studies of nanoconfined water dynamics have given conflicting results ranging from liquidlike to solidlike behavior. Direct SFA measurements [8,9] and simulations [10,11] have shown that water and aqueous solutions maintain the viscosity of bulk water down to nanometer-scale confinement. However, similar measurements have shown that the shear viscosity increases by orders of magnitude [12–15], and simulations have indicated an increase in the translational and rotational correlation lifetimes [16,26]. Computational models of water demonstrate a rich phase behavior consistent with solidification [17–19] and dynamical phenomena like shear thinning [10,20] and shear melting and freezing [16].

The reconstructed behavior of nanoconfined water for $D = 9.2$ Å at the initiation of shear (0 fs) is shown in Fig. 4(a). White regions in the contour plots denote "bulklike water" regions, defined as regions with no density difference from bulk water. Enhancements in oxygen density are represented by progressive shading from light yellow to dark red for increasingly positive values. Depletion of oxygen density is
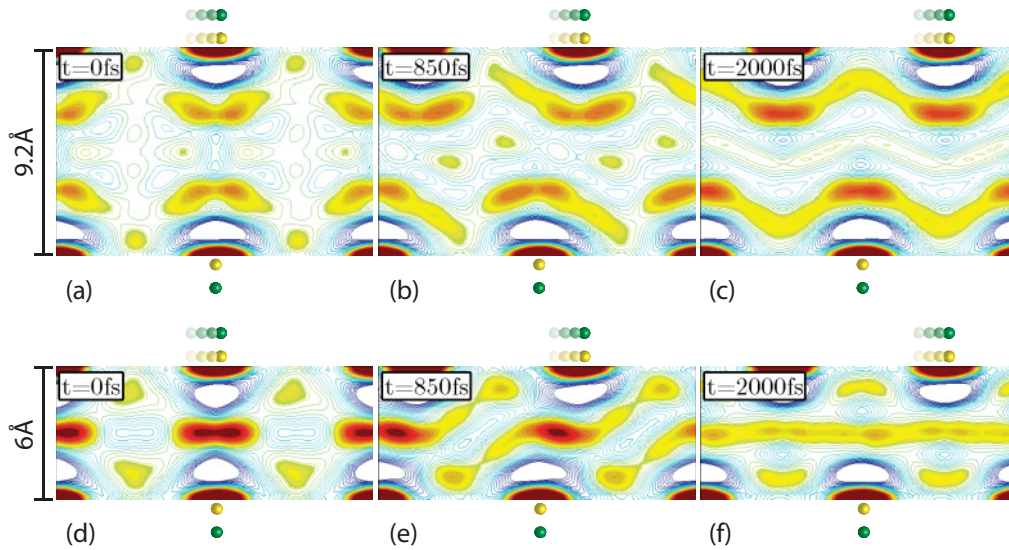
FIG. 4. (Color online) The time-dependent density profile for confined water in the XZ plane containing the surface dipoles on each sheet. The top sheet is shearing with velocity V in the X direction, Z is the direction of confinement, and these densities are integrated from a 2-Å slab in the Y direction centered on the dipoles. For $D = 9.2$ Å, the *in registry* hydration structure of the confining surfaces (a) is characterized by bulklike water sandwiched between well-defined surface-structured hydration layers. As the top surface is sheared at $V = 200$ m/s (b), (c), the hydration layers are distorted and exhibit cycles of deformation and recovery as the dipole sites on the top and bottom surfaces move into and out of registry. For the $D = 6$ Å case, the two hydration structures are forced to reconstruct into one. When the surfaces are in registry (d), the confined water has a highly localized structure. As the top surface is sheared, the hydration structure deforms to bridge the two surfaces (e). When the surfaces are out of registry, the water in the center of the channel appears to be "shear melted," with densities close to that of bulk water (f). The hydration returns to the well-defined structure (d) as the interaction sites come into registry again.

represented by open dark blue contours. Hydration at the two surfaces is clearly coupled, but only weakly. Water is known to exhibit fast dynamics and is expected to equilibrate to changing boundary conditions quickly. When subjected to shear ($V = 200$ m/s), the hydration structure becomes distorted away from the $v = 0$ "static" hydration structure with a degree of distortion that is dependent on v. That a modified form of hydration structures persists indicates that the water can equilibrate quickly around hydration sites at the present shear rates. Moreover, the confined hydration structures exhibit cycles of deformation and recovery as the oxygen density accommodates the changing boundary conditions [Figs. 4(b) and 4(c)]. Importantly, between the hydration layers associated with the top and bottom surfaces, there exists a bulklike layer of water without significantly altered density. Bulk fluidity is expected as these layers are sheared even at 9.2-Å intersurface separation. This behavior is generic for a broad range of shear speeds in our reconstructions.

The situation is qualitatively different when the intersurface separation is decreased slightly to $D = 6$ Å. The two hydration layers associated with the top and bottom confining surfaces reconstruct into a single composite layer that alternates between two different structures. When the dipoles on the two confining surfaces are in registry [Fig. 4(d)], a strong hydration structure is observed. The two-dimensional nature is reminiscent of "monolayer ice" observed in water confined in subnanometer gaps, but the lattice constant and symmetry templated by the surface are distinct from that of ice [17]. When the dipoles on the two surfaces become out of registry [Figs. 4(e) and 4(f)] we observe a delocalized, "melted" structure. This is characterized by a nearly constant, featureless layer of enhanced oxygen

density in place of the localized bridging oxygen found for the in-registry case. Under continued shearing cycles, the system transitions between these localized frozen and delocalized melted structures. These transitions constitute the hydrophilic analog to transitions observed in simulations of water confined in hydrophobic nanometer gaps [17,18,33]. The emergence of strong "bridging" oxygen density between the confining surfaces (reminiscent of "stick-slip" phenomena) under these shearing conditions is consistent with the observation of an increase in shear viscosity for a monolayer of hydration between mica sheets [13]. These drastic changes in our reconstructions as the confinement gap is changed by ∼3 Å is interesting and potentially reconciles results from direct measurements [8–11,13,15,16,34]. In experiment with real surfaces, we would expect some deviation due to surface chemistry and the binding of the first water layer. However, the distances we find here are largely determined by the structure of water itself, such as the characteristic oxygen-oxygen distance and the size of the water molecule, length scales that are ultimately expressed in the surface-induced layering of water.

Interestingly, when we vary the dipole density on the confining hydrophilic surfaces, we find an unanticipated delocalized wetting regime for nanoconfined water. Under these conditions, water is strongly resistant to "freezing" down to intersurface separations at molecular distances (<6 Å). As the dipole densities on our model confining surfaces are increased, an increase in nanoconfined water ordering may be expected. The opposite is found instead. We examined a series of reconstructions, each with a different, fixed interdipole spacing a. For $D = 6$ Å and $a = 3.5$ Å, the strong hydration
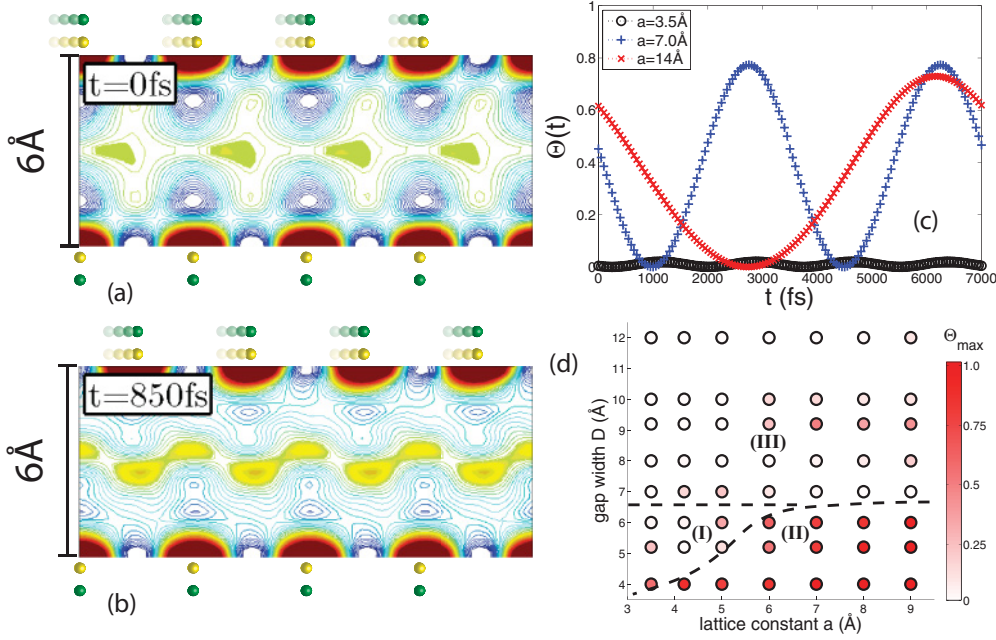
FIG. 5. (Color online) The (a) in-registry and (b) out-of-registry hydration structure in the $D = 6$ Å confining gap between square lattice ($a = 3.5$ Å) hydrophilic surfaces. The top surface is sheared at $v_x = 200$ m/s to compare to the $a = 7$ Å case. The increase in interaction site density eliminates the dynamical formation of dense, localized hydration structures as seen for lower site density cases. (c) The order can be quantified by comparing the density structure factor $S_{\text{center}}(k = \mathbf{k}_1)$ in the center of the gap to the structure factor of adhered hydration structure at the stationary surface $S_{\text{adhesion}}(k = \mathbf{k}_1)$, where $\mathbf{k}_1$ is the reciprocal lattice vector in the direction of shear ($|\mathbf{k}_1| = 2\pi/a$). For large surface lattice spacing ($a = 14$ Å, $a = 7$ Å), the order ratio $\Theta = S_{\text{center}}(\mathbf{k}_1)/S_{\text{adhesion}}(k = \mathbf{k}_1)$ shows periodic oscillation between $\Theta = 0$, indicating complete delocalization of water density in the XY plane, and $\Theta = 0.8$, indicating that the hydration structure in the gap is nearly as ordered as it is at the stationary interface. As the interaction site density is increased ($a = 3.5$ Å), $\Theta \approx 0$ at all times. (d) The maximum order ratio Θ_{max} during shear for different values of D and a is represented in a dynamical phase diagram for confined water. For subnanometer gaps and high interaction site density (region I), the hydration structure induced is in a constant delocalized state of frustrated liquidlike water. The freeze-melt transition regime (region II) occurs for lower interaction site densities and small gaps ($D \approx 10$ Å). For large gaps ($D \geqslant 10$ Å, region III), the surfaces have little effect in the middle of the gap ($\langle \delta\rho^2 \rangle \approx 0$), resulting in bulklike water between single-surface hydration structures. This crossover occurs for gap distances D that permit more than three layers of water molecules (two adhered layers and one shared first hydration layer).

structures no longer appear when the dipole sites are in registry [Fig. 5(a)] as they do for the $a = 7$ Å case [Fig. 4(d)]. Furthermore, there is little time dependence on the evolution of induced oxygen density [Figs. 5(a) and 5(b)]. Competition between dipole sites on a surface frustrates the hydration process. For lattice constants comparable to the intermolecular water spacing ($a \approx r_{\text{OO}} = 2.8$ Å), the surface dipole density is too high for each to have independent hydration structures. Instead, the array is wetted by a delocalized layer of water. Essentially, the transition between discrete hydration structures localized around individual dipoles and a frustrated, delocalized hydration layer occurs when $a/r_{\text{OO}} \approx 1$, where r_{OO} is the natural "wavelength" of water density fields (the O-O distance) and a is the "mean distance" between interaction sites [35]. These effects can be quantified in a dynamical phase diagram. In this phase diagram, we computationally examine seven types of surfaces for our two confining plates, each of which is decorated with a different dipole density. For each of these situations, we generated movies for eight different the interplate spacings (gap widths) between 4 and 12 Å. The range of dipole densities thus examined spans the range found in real surfaces such as mica.

IV. DISCUSSION

In each of the movies, we compare the structure factor of the fluid layer in the center of the channel, $S_{\text{center}}(k)$, to that of the layer of adhered water on the stationary surface, $S_{\text{adhered}}(k)$, at the reciprocal lattice vector $\mathbf{k}_1$ corresponding to the interaction site periodicity in the direction of shearing, $|\mathbf{k}_1| = 2\pi/a$ [Figs. 5(c) and 5(d)]. This structure factor ratio $\Theta = S_{\text{center}}(\mathbf{k}_1)/S_{\text{adhered}}(\mathbf{k}_1)$ approaches 1 if the hydration in the center is as localized as that at the interface, and is 0 when it is purely delocalized. Similar metrics have been used to demonstrate shear melting in simulations [10,36]. Figure 5(c) shows that for large dipole spacings ($a > r_{\text{OO}}$) the order ratio $\Theta(t)$ oscillates between ~ 0.8 as the dipole sites are in registry across the gap, and ~ 0 as they are out of registry. This oscillation has a period of $T = a/v_x$ for the square lattices studied here. For small dipole spacings ($a \sim r_{\text{OO}}$), Θ is much less than 1 at all times, indicating that water in the gap is never strongly ordered under these shearing conditions. In other words, surfaces with high densities of weak dipoles organize water into a delocalized hydration layer that is strongly resistant to the formation of "bridging" oxygen density between the confining surfaces even at nanoscopic

interplate distances. The application of the bulk response function to nanoconfinement suggests that water has a strong tendency to maintain fluidity down to subnanometer-scale gaps in systems with high spatial frequency of charge modulations [37]. The reconstructions indicate that surfaces exhibit two distinct forms of hydrophilic hydration, one where the water hydrogen bonding network is tethered onto a surface via discrete anchoring points localized to hydration sites, and one where water is "glued" to a surface via an incommensurate delocalized hydration layer. This result has interesting implications to lubrication, especially in biological and biomimetic systems [37–39]. These interpretations could be clarified further by molecular dynamics (MD) simulations of similar shearing geometries.

The femtosecond movies above suggest explanations for nanoconfined water behavior. For large gaps ($D > 10$ Å), the surface has little influence on the hydration structure in the center of the gap, leading to bulklike shear dynamics. For smaller gaps that accommodate only the first cohesive hydration layer ($D/r_{OO} < 3$), the mean-squared density fluctuations are large ($\langle \Delta^2 \rho \rangle > 0$), indicating that the surface has a strong influence on the hydration structure throughout the gap. These results can be understood in terms of interference between density fields. The Green's function creates phonons with a coherence length of ~ 1 nm. Phonons lose phase information as they propagate away from the solid surface and become progressively unable to exhibit coherent interference, until eventually all memory of the solid surface is lost. If interaction sites are within the coherence length of the Green's function, as seen most clearly in the $D = 6$ Å case,

their hydration structures can coherently interfere to generate localized and delocalized hydration structures. For confining surfaces positioned farther apart than the coherence length, these interference effects are lost as phonons dephase and decay into heat as they interact with their environment in a thermodynamically irreversible manner, so that bulklike liquid water exists midgap. Localized and delocalized density in the gap has a strong influence on the landscape of diffusional dynamics in the xy plane, leading to behavior that mimics liquidlike low-viscosity and solidlike high-viscosity behavior.

In summary, we have extracted the density propagator of water from IXS measurements and used it to reconstruct the behavior of water near hydrophilic surfaces and of water confined between hydrophilic surfaces. The results agree with extant experimental and computational work and reproduce parameters such as the decay length of surface-induced water layering. We find that the transition between fluid- and solidlike water under nanoconfinement can be understood in terms of interference phenomena between surface-induced density fields. Finally, our results suggest that there are two qualitatively distinct types of hydrophilic surfaces, each with a different behavior under nanoconfinement.

[1] B. de Groot and H. Grubmuller, Science **294**, 2353 (2001).

[2] E. Tajkhorshid, P. Nollert, M. O. Jensen, L. Miercke, J. O'Connell, R. M. Stroud, and K. Schulten, Science **296**, 525 (2002).

[3] S. Karaborni, B. Smit, W. Heidug, J. Urai, and E. van Oort, Science **271**, 1102 (1996).

[4] E. Hensen and B. Smit, J. Phys. Chem. B **106**, 12664 (2002).

[5] B. Bhushan, J. Israelachvili, and U. Landman, Nature (London) **374**, 607 (1995).

[6] M. Urbakh, J. Klafter, D. Gourdon, and J. Israelachvili, Nature (London) **430**, 525 (2004).

[7] B. Bagchi, Chem. Rev. **105**, 3197 (2005).

[8] U. Raviv, P. Laurat, and J. Klein, Nature (London) **413**, 51 (2001).

[9] U. Raviv and J. Klein, Science **297**, 1540 (2002).

[10] Y. Leng and P. Cummings, Phys. Rev. Lett. **94**, 026101 (2005).

[11] C. Sendner, D. Horinek, L. Bocquet, and R. Netz, Langmuir **25**, 6830 (2009).

[12] A. Dhinojwala and S. Granick, J. Am. Chem. Soc. **119**, 241 (1997).

[13] Y. Zhu and S. Granick, Phys. Rev. Lett. **87**, 096104 (2001).

[14] H. Sakuma, K. Otsuki, and K. Kurihara, Phys. Rev. Lett. **96**, 046104 (2006).

[15] T.-D. Li, J. Gao, R. Szoszkiewicz, U. Landman, and E. Riedo, Phys. Rev. B **75**, 115415 (2007).

[16] Y. Leng and P. Cummings, J. Chem. Phys. **125**, 104701 (2006).

[17] R. Zangi and A. Mark, Phys. Rev. Lett. **91**, 025502 (2003).

[18] R. Zangi and A. Mark, J. Chem. Phys. **119**, 1694 (2003).

[19] P. Feibelman, Phys. Today **63**, 34 (2010).

[20] A. Malani, K. Ayappa, and S. Murad, J. Phys. Chem. B **113**, 13825 (2009).

[21] R. Coridan, N. Schmidt, G. Lai, R. Godawat, M. Krisch, S. Garde, P. Abbamonte, and G. Wong, Phys. Rev. Lett. **103**, 237402 (2009).

[22] R. Coridan, N. Schmidt, G. Lai, and G. Wong, J. Phys. Condens. Matter **21**, 424115 (2009).

[23] R. H. Coridan and G. C. Wong, *Advances in Chemical Physics*, Chap. 3 (Wiley, New York, 2012).

[24] A. Patel, P. Varilly, and D. Chandler, J. Phys. Chem. B **114**, 1632 (2010).

[25] L. Cheng, P. Fenter, K. Nagy, M. Schlegel, and N. Sturchio, Phys. Rev. Lett. **87**, 156103 (2001).

[26] Y. Leng and P. Cummings, J. Chem. Phys. **124**, 074711 (2006).

[27] Y. Liu, D. Berti, P. Baglioni, S.-H. Chen, A. Alatas, H. Sinn, A. Said, and E. Alp, J. Phys. Chem. Solids **66**, 2235 (2005).

[28] T. Angelini, R. Golestanian, R. Coridan, J. Butler, A. Beraud, M. Krisch, H. Sinn, K. Schweizer, and G. Wong, Proc. Natl. Acad. Sci. USA **103**, 7962 (2006).

[29] P. Abbamonte, K. Finkelstein, M. Collins, and S. Gruner, Phys. Rev. Lett. **92**, 237401 (2004).

[30] P. Abbamonte, G. Wong, D. Cahill, J. Reed, R. Coridan, N. Schmidt, G. Lai, Y. Joe, and D. Casa, Adv. Mater. **22**, 1141 (2010).

[31] D. Pines and P. Nozieres, *The Theory of Quantum Liquids*, Vol. 1 (Benjamin, New York, 1966).

[32] T. Fukuma, Y. Ueda, S. Yoshioka, and H. Asakawa, Phys. Rev. Lett. **104**, 016101 (2010).

[33] N. Giovambattista, P. Rossky, and P. Debenedetti, Phys. Rev. Lett. **102**, 050603 (2009).

[34] M. Goertz, J. Houston, and X. Zhu, Langmuir **23**, 5491 (2007).

[35] This is analogous to the Ioffe Regel criterion in solid state physics.

[36] P. Thompson and M. Robbins, Science **250**, 792 (1990).

[37] M. Chen, W. Briscoe, S. Armes, and J. Klein, Science **323**, 1698 (2009).

[38] J. Gong, Soft Matter **2**, 544 (2006).

[39] L. Han, D. Dean, P. Mao, C. Ortiz, and A. Grodzinsky, Biophys. J. **93**, L23 (2007).